Bioactive Materials 40 (2024) 683–695

Contents lists available at ScienceDirect

Bioactive Materials

journal homepage: www.keaipublishing.com/en/journals/bioactive-materials

High throughput and rapid isolation of extracellular vesicles and exosomes with purity using size exclusion liquid chromatography

Kshipra S. Kapoor [a,b], Kristen Harris [a], Kent A. Arian [a], Lihua Ma [c], Beatriz Schueng Zancanela [a], Kaira A. Church [a], Kathleen M. McAndrews [a], Raghu Kalluri [a,c,d,*]

[a] Department of Cancer Biology, Metastasis Research Center, University of Texas MD Anderson Cancer Center, Houston, TX, USA
[b] Department of Electrical and Computer Engineering, Rice University, Houston, TX, USA
[c] Department of Bioengineering, Rice University, Houston, TX, USA
[d] Department of Molecular and Cellular Biology, Baylor College of Medicine, Houston, TX, USA

ARTICLE INFO

Keywords:
Extracellular vesicles
Size exclusion - fast performance liquid chromatography
Isolation methods

ABSTRACT

Extracellular vesicles (EVs) have emerged as potential biomarkers for diagnosing a range of diseases without invasive procedures. Extracellular vesicles also offer advantages compared to synthetic vesicles for delivery of various drugs; however, limitations in segregating EVs from other particles and soluble proteins have led to inconsistent EV retrieval rates with low levels of purity. Here, we report a new high-yield (88.47 %) and rapid (<20 min) EV isolation method termed size exclusion – fast protein liquid chromatography (SE-FPLC). We show SE-FPLC can effectively isolate EVs from multiple sources including EVs derived from human and mouse cells and serum samples. The results indicate that SE-FPLC can successfully remove highly abundant protein contaminants such as albumin and lipoprotein complexes, which can represent a major hurdle in large scale isolation of EVs. The high-yield nature of SE-FPLC allows for easy industrial scaling up of EV production for various clinical utilities. SE-FPLC also enables analysis of small volumes of blood for use in point-of-care diagnostics in the clinic. Collectively, SE-FPLC offers many advantages over current EV isolation methods and offers rapid clinical translation.

1. Introduction

Advanced Therapeutic Medicinal Products (ATMPs) provide innovative approaches for designing solutions for diagnosing and combating complex diseases [1,2]. Promising breakthroughs in cutting-edge technologies, such as chimeric antigen receptor (CAR)-T cells [3–5] and mRNA vaccines [6–9], illustrate the potential of such unconventional thinking. These success stories demonstrate the utility of ATMPs and the need to explore novel therapeutic solutions for unmet medical needs. Extracellular vesicles (EVs) contain molecular cargo such as: proteins, nucleic acids, lipids, and metabolites reflecting their cell of origin [10–12]. EV membranes harbor lipid rafts characterized by high concentrations of cholesterol, sphingomyelin and ceramide, rendering them highly stable in body fluids and hence making them appealing for therapeutic purposes [13]. EVs also contain major histocompatibility complexes and can engage with the immune system in various antigen-specific ways [14]. Considering these benefits, EVs offer a promising platform for therapeutic development and in many cases, they can be engineered to enhance their therapeutic potential thereby making them a versatile tool with broad applicability [15–18]. EVs have also garnered attention as potential disease biomarkers in liquid biopsy for cancer [19] and neurological diseases [20], among others. As EVs carry a diverse range of molecular cargo, they can serve as important biosignatures for disease diagnosis and therapeutic intervention. The potential diagnostic [21] and therapeutic applications [22] of EVs highlights the importance for developing new protocols for their rapid isolation with purity to enable continued laboratory investigations and development as a valuable tool in disease management; however, the production of EVs, especially at an industrial scale, still represents a significant challenge, including product definition, low purity, and low yields [23–25]. Additionally, the lack of standardized EV isolation methods and the limited scalability of existing protocols for preparative purposes beyond the laboratory scale further compound these challenges. Therefore, our objective was to develop a scalable and

Peer review under responsibility of KeAi Communications Co., Ltd.
* Corresponding author.
E-mail address: rkalluri@mdanderson.org (R. Kalluri).

https://doi.org/10.1016/j.bioactmat.2024.08.002
Received 1 May 2024; Received in revised form 31 July 2024; Accepted 2 August 2024

reproducible method that meets the demands to produce pure EVs.

A recent literature survey reveals that there are around 190 different methods reported for isolating EVs and over 1000 unique protocols for extracting EVs from various sources of origin [26]. Differential ultracentrifugation (dUC) [27] continues to be the most frequently employed method for isolating EVs; however, this method necessitates lengthy protocols, limited by ultracentrifuge tube capacity in the case of bulk isolation and often involves a trade-off between EV yield and purity [27–30]. Other approaches [31–36] to EV isolation, such as polymer precipitation and immunoaffinity capture, have been explored to address the limitations of traditional methods, offering simplified procedures and shorter isolation times. However, polymer precipitation is prone to co-isolation of contaminating proteins, which can interfere with downstream analysis. Likewise, immunoaffinity capture methods may only isolate a subset of EVs, which introduces potential bias in the subsequent analysis [37]. While an alternative approach that avoids this potential limitation is utilizing bind-elute affinity chromatography for EV separation [38], such an approach requires altering solvent conditions that can result in biological and chemical instability of biologics. These limitations underscore the need for a rigorous exploration of alternative EV isolation methods to ensure rapid and optimal results [39,40].

This study presents a new ultrafast purification technique, size exclusion – fast protein liquid chromatography (SE-FPLC), for EV isolation that overcomes the limitations of other methods. To confirm the SE-FPLC, we performed measurements on the isolated EV samples and address different published guidelines (MISEV2018) [41] in the EV field. We thoroughly characterized the obtained EV fractions for enrichment of EV-specific markers and absence of non-EV proteins. To verify the EV purity standard protein detection methods were employed, size distribution was analyzed by nanoparticle tracking analysis (NTA), and EV morphology was imaged by cryo-EM imaging. We compared the SE-FPLC performance with dUC, density gradient and small-scale size exclusion chromatography, and overall, SE-FPLC exhibited enhanced speed, yield and purity. We show that SE-FPLC delivers superior results with reduced processing time thereby aiding better economics and a lower carbon footprint.

2. Results

2.1. Development and characterization of SE-FPLC for high purity EV isolation

To achieve fast, efficient and pure EV isolation, we developed a SE-FPLC methodology that separates EVs based on size. We investigated the EV purification utilizing the AKTA pure 25 chromatography system (Cytiva) in conjunction with a size exclusion chromatography column capable of processing up to 100 mL sample loading volume (IZON qEV10). To characterize the separation efficiency, we isolated EVs with a particle diameter below 200 nm from different cell lines representing different origins: malignant epithelial cancer cells (Panc1 and T3M4), bone marrow mesenchymal stem/stromal cells (MSCs), foreskin fibroblasts (BJ fibroblast) and non-malignant epithelial cells (HEK293T). The UV absorption spectra at wavelength 280 nm revealed two peaks, an EV-enriched peak and a protein enriched peak, from distinct elution fractions for all cell lines tested (Fig. 1A–D, Supplementary Figs. S1A–K). To ensure that maintenance in serum-free medium for EV harvesting did not negatively affect cell viability, we used a trypan blue exclusion assay that allows for direct identification and enumeration of live and dead cells (Supplementary Fig. S1L). We observed low cellular death in the cells cultured in serum-free media for EV isolation (Supplementary Fig. S1L).

We further evaluated the presence of EV and non-EV markers in SE-FPLC fractions by western blot analysis. CD81, CD9 and syntenin-1 [42] were used as EV markers and the glycolytic enzyme GAPDH and DNA binding protein histone H3 were employed as non-EV markers respectively (Fig. 1). Additionally, we used the non-EV marker GM130 (Supplementary Fig. 1M). Equal-sample-volume analysis (45 μL) was used to characterize fractions for the presence of EV markers. In each of the cell line isolated EVs, we detected putative EV marker proteins in the fractions corresponding to the first elution peak (EV-enriched, Fig. 1E–L). Further, the non-EV markers were absent in the fractions corresponding to the first peak of elution and were significantly enriched in fractions corresponding to the second peak of elution (PRO-enriched, Fig. 1E–L) and a cell lysate control (Supplementary Fig. 1M) thereby indicating effective separation of EVs from non-EV associated proteins.

The main performance metrics considered in this study were the processing time, EV purity and total yield. While most of the current protocols require at least 8 h to isolate the samples, the SE-FPLC approach can be performed in as little as 18 min with a 1-h total processing time including the pre-processing centrifugation and filtration steps common to all other isolation approaches (Fig. 2A). Coomassie and silver staining of proteins further confirmed that SE-FPLC removed most protein contaminants across all model systems (Fig. 2B–E and Supplementary Figs. S2A–B). We validated the isolation method by re-isolating the recovered EV-rich fraction with SE-FPLC and found that approximately 99 % of protein was removed and 88.47 % of EVs were recovered in the first peak of elution (Supplementary Figs. S2C–E). NTA also showed minimal particles detected in the PRO-enriched fractions in contrast to the EV-enriched fractions (Supplementary Fig. S2E). Furthermore, EV isolation from MSCs (Supplementary Fig. 3) and Panc1 cells (Supplementary Fig. 4) via gold standard techniques such as differential ultracentrifugation (dUC), density gradient (DG) and small-scale size exclusion chromatography (SEC) results in lower yield compared the SE-FPLC isolation method (Supplementary Figs. S3A–E and Supplementary Figs. S4A–D). EVs isolated by various isolation methods displayed a similar size of approximately 40–200 nm (Supplementary Fi gure S3A-C, S4A-C). Imaging with cryogenic electron microscopy (cryo-EM) also showed Panc1 EVs with similar size and morphology, independent of isolation method (Fig. 2F and Supplementary Figs. S4E–H). Overall, the SE-FPLC technology demonstrated increased purity and growth potential with reduced time and energy requirements and lower technology complexity (Fig. 2G).

2.2. SE-FPLC for rapid EV isolation exhibits growth potential and high reproducibility

Next to evaluate the reproducibility and growth potential of SE-FPLC, we processed independent biological replicates of Panc1, T3M4 and MSC EVs. The UV–Vis absorbance spectra indicated good reproducibility of SE-FPLC (Supplementary Figs. S1A–K). We isolated MSC-derived EVs by SE-FPLC and measured the protein concentration (μg/mL) in EV-enriched peak fractions and PRO-enriched peak fractions (Supplementary Figs. S5A–C). The coefficient of variation of the measurements for the ratio of EV-enriched peak fractions and PRO-enriched peak fractions was 16.4 %, thereby indicating effective reproducibility of SE-FPLC.

2.3. SE-FPLC method facilitates albumin depletion and removal of lipoproteins

Enriching for EVs while effectively excluding highly abundant free proteins such as albumin and lipoproteins of similar density, such as high-density lipoprotein particles (HDLs), poses a significant technical challenge given the relatively low abundance of EVs and similar size and density compared to free proteins and lipoproteins in certain biological samples [43,44]. We assessed the capability of SE-FPLC to enrich EVs from both free proteins (albumin) and lipoproteins (Apo-LipoA1, a component of HDL). Our SE-FPLC approach aided in albumin depletion in as little as 18 min, whereas commercially available albumin-depletion kits take over 1 h and 30 min for the removal of albumin from serum

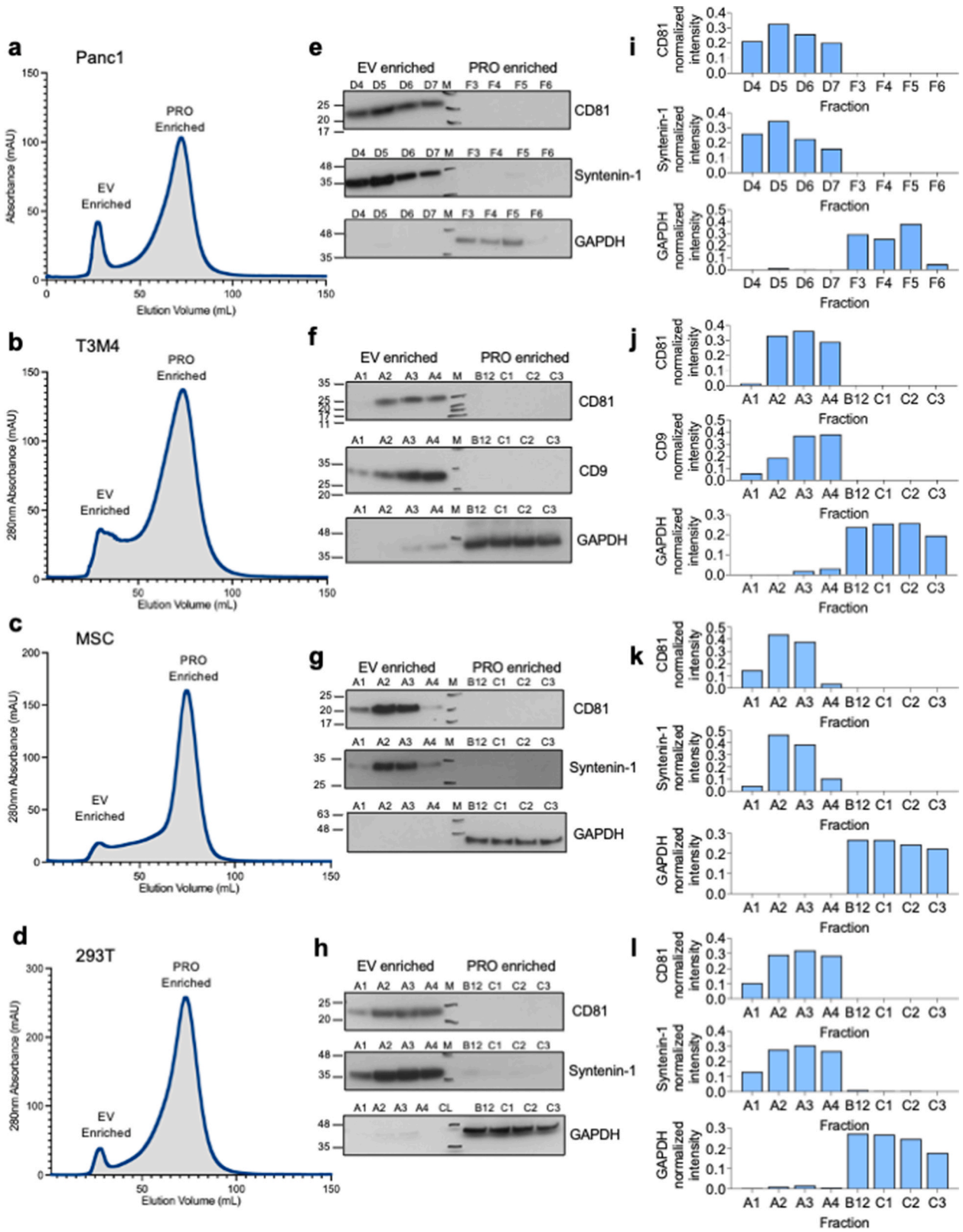

Fig. 1. Characterization of SE-FPLC performance. (**A-D**) Representative UV–Vis chromatographs for EV isolation from Panc1 (**A**), T3M4 (**B**), MSC (**C**), and 293T (**D**) conditioned media. (**E-H**) Presence of EV inclusion (CD81, CD9 and syntenin-1) and exclusion markers (GAPDH and histone H3) in SE-FPLC fractions characterized by western blot for Panc1 (**E**), T3M4 (**F**), MSC (**G**) and 293T (**H**). The fractions analyzed are indicated above each lane, M denotes the molecular weight marker and CL denotes cell lysate. (**I-L**) Quantification of band intensities for respective fractions is shown in the right panel for Panc1 (**I**), T3M4 (**J**), MSC (**K**) and 293T (**L**). The normalized intensity quantification of the western blot band was analyzed by ImageJ. Data are presented as individual values in each plot.

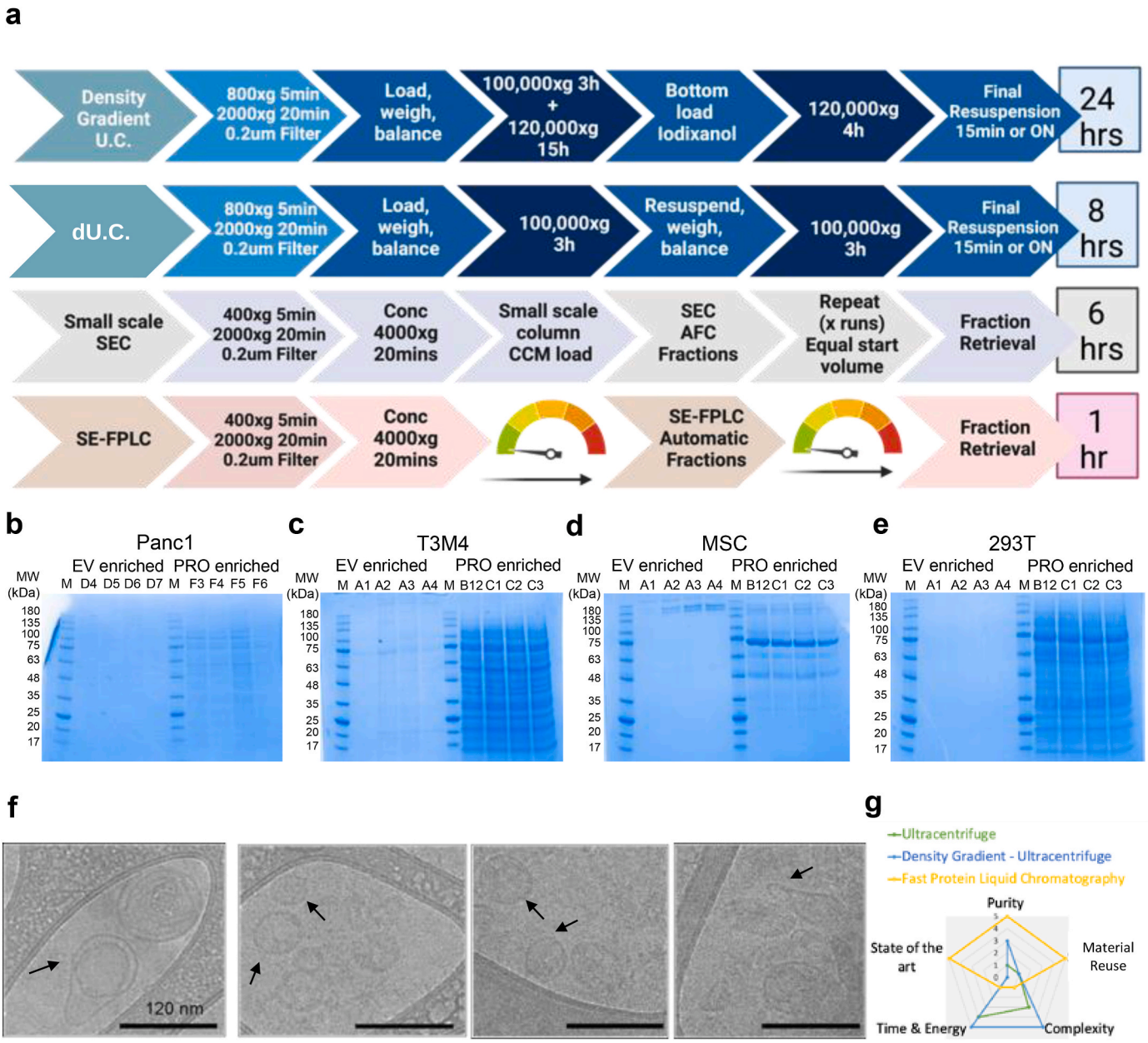

Fig. 2. Characterization of SE-FPLC performance and processing time comparison to other methods of EV isolation. (**A**) Comparison between density gradient ultracentrifugation (DG-UC), differential ultracentrifugation (dUC), small scale size exclusion chromatography (SEC) and size-exclusion fast protein liquid chromatography (SE-FPLC) detailed procedures and sample processing times. (**B-E**) Equal-sample-volume analysis (45 μL) of total proteins in each fraction by Coomassie staining for Panc1 (**B**), T3M4 (**C**), MSC (**D**) and 293T (**E**) EVs isolated by SE-FPLC. The fractions analyzed are indicated above each lane and M denotes the molecular weight marker. (**F**) Cryogenic electron microscopic images of EVs isolated from mesenchymal stem cells using SE-FPLC. Scale bars, 120 nm. (**G**) Two-dimensional comparison of scalability, time and energy, purity and state-of-the art of SE-FPLC and other EV isolation methods.

(Fig. 3A–B). To determine if the albumin depletion was successful, we quantified albumin levels in both EV-enriched and PRO-enriched fractions across multiple model systems and found specific detection of albumin in PRO-enriched fractions (Fig. 3C–E). Our approach greatly improved the albumin-depletion process for purification of EVs, thereby potentially improving various downstream analysis.

EVs have been reported to have similar density as small HDL particles both belonging in the range of 1.05–1.21 g/mL (Fig. 3F). Thus, due to the similar densities there are high chances of co-isolating both EVs and HDL particle populations using traditional approaches such as density gradient ultracentrifugation [43,45–47]. SE-FPLC approach demonstrated the ability to separate HDL and EV particles in one-step due to size differences (5–10 nm compared to 50–220 nm, respectively). Dimerized Apo-Lipo A1 was enriched in the PRO-enriched fractions (Fig. 3G) hence confirming the SE-FPLC partitions HDL particles in the non-EV enriched fractions away from the purified EV population.

2.4. Isolation of serum EVs via SE-FPLC

To determine the versatility of SE-FPLC, we evaluated the ability to isolate and purify EVs from human serum. Serum-derived EVs can function as liquid biopsies for monitoring disease-associated changes as they are released into the bloodstream from their cells of origin in the tissue [48]. We isolated EVs from healthy serum samples using SE-FPLC (demographic data for the samples are reported in Supplementary Table

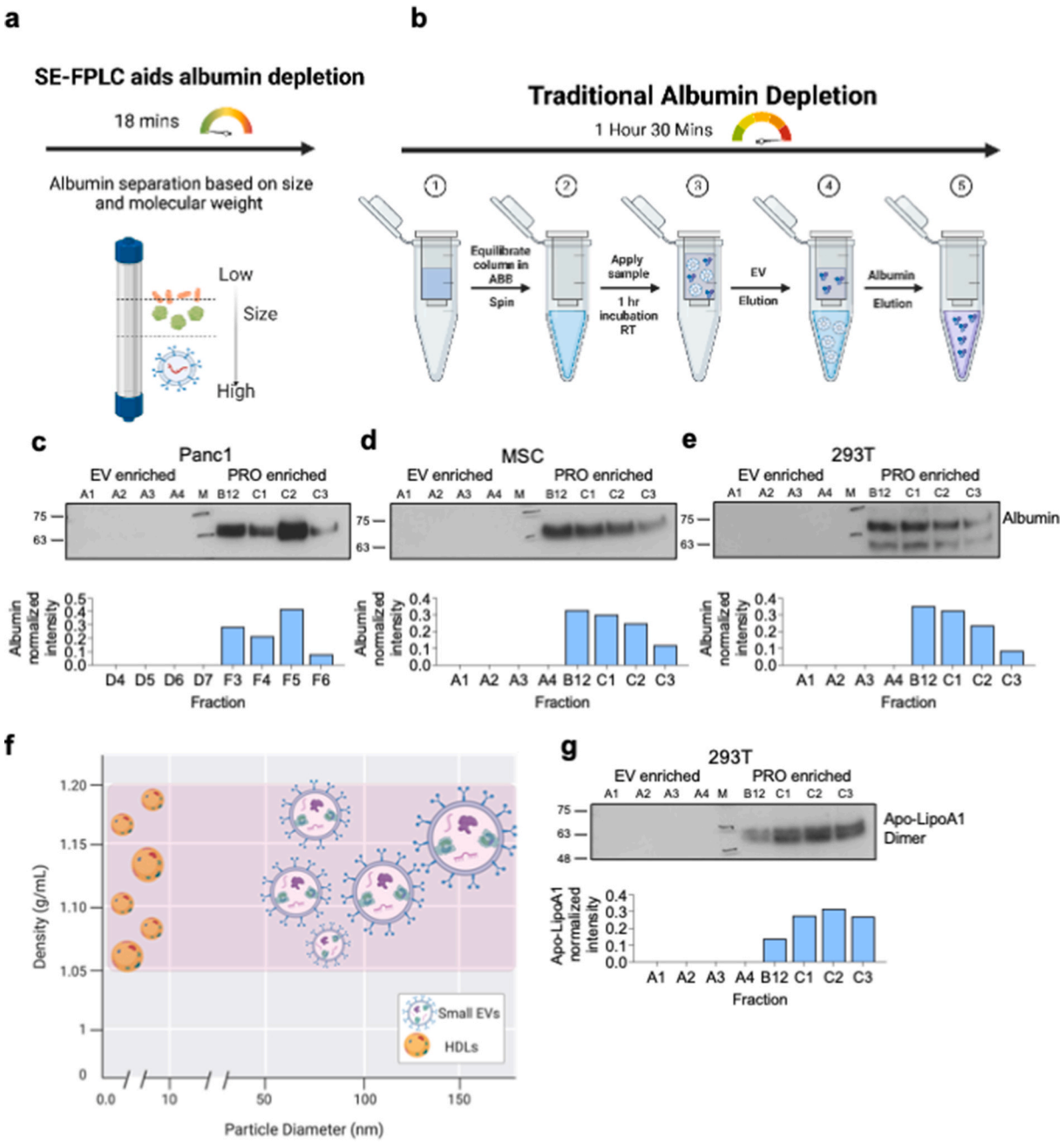

Fig. 3. SE-FPLC method facilitates albumin depletion and removal of lipoprotein complexes. (A) Schematic of albumin depletion in one-step and processing time via the SE-FPLC method. **(B)** Schematic of traditional albumin depletion procedure and the traditional protocol processing time. (**C-E**) EV samples were isolated by SE-FPLC approach and equal-sample volumes (45 μL) of each fraction were analyzed by western blot analysis for presence of albumin in Panc1 (**C**), MSC (**D**), and 293T (**E**) derived EVs. The fractions analyzed are indicated above each lane and M denotes the molecular weight marker. The normalized intensity quantification of the western blot band was analyzed by ImageJ and is shown below each respective blot. (**F**) Comparison of density (g/mL) and particle diameter (nm) of high-density lipoprotein (HDL) particles and small extracellular vesicles (sEVs). (**G**) Western blot analysis (top) and quantification (bottom) of Apo-LipoA1 in SE-FPLC fractions from 293T derived EVs. The fractions analyzed are indicated above each lane and M denotes the molecular weight marker. Data are presented as individual values in each plot.

1). The UV–Vis absorbance spectra of healthy donor samples revealed the ability to detect a minor EV-enriched peak separate from prevalent serum proteins (Fig. 4A). Due to high-yield and high-purity, SE-FPLC reduced biofluid starting volume requirements to 500 μL. The serum EVs isolated by SE-FPLC were further inspected by cryo-EM (Supplementary Figs. S6A–F). The majority of the serum isolated EVs were between 40 and 200 nm, with approximately 70 % of single-molecule independent EVs were in size range between 30 and 140 nm and approximately 25 % of the single-molecule independent EVs ranged between 150 and 220 nm (mean ± SD = 118.687 ± 67.142) (Supplementary Fig. S6G).

2.5. *Detection of mutant KRAS in SE-FPLC isolated EVs from pancreatic cancer cell lines*

To highlight the performance for practical cancer applications of SE-FPLC, we isolated EVs from pancreatic ductal adenocarcinoma (PDAC) murine (KPC689) and human (Panc1) cell lines using SE-FPLC (Fig. 4B). KPC689 EV-enriched fractions showed enrichment of CD81, whereas

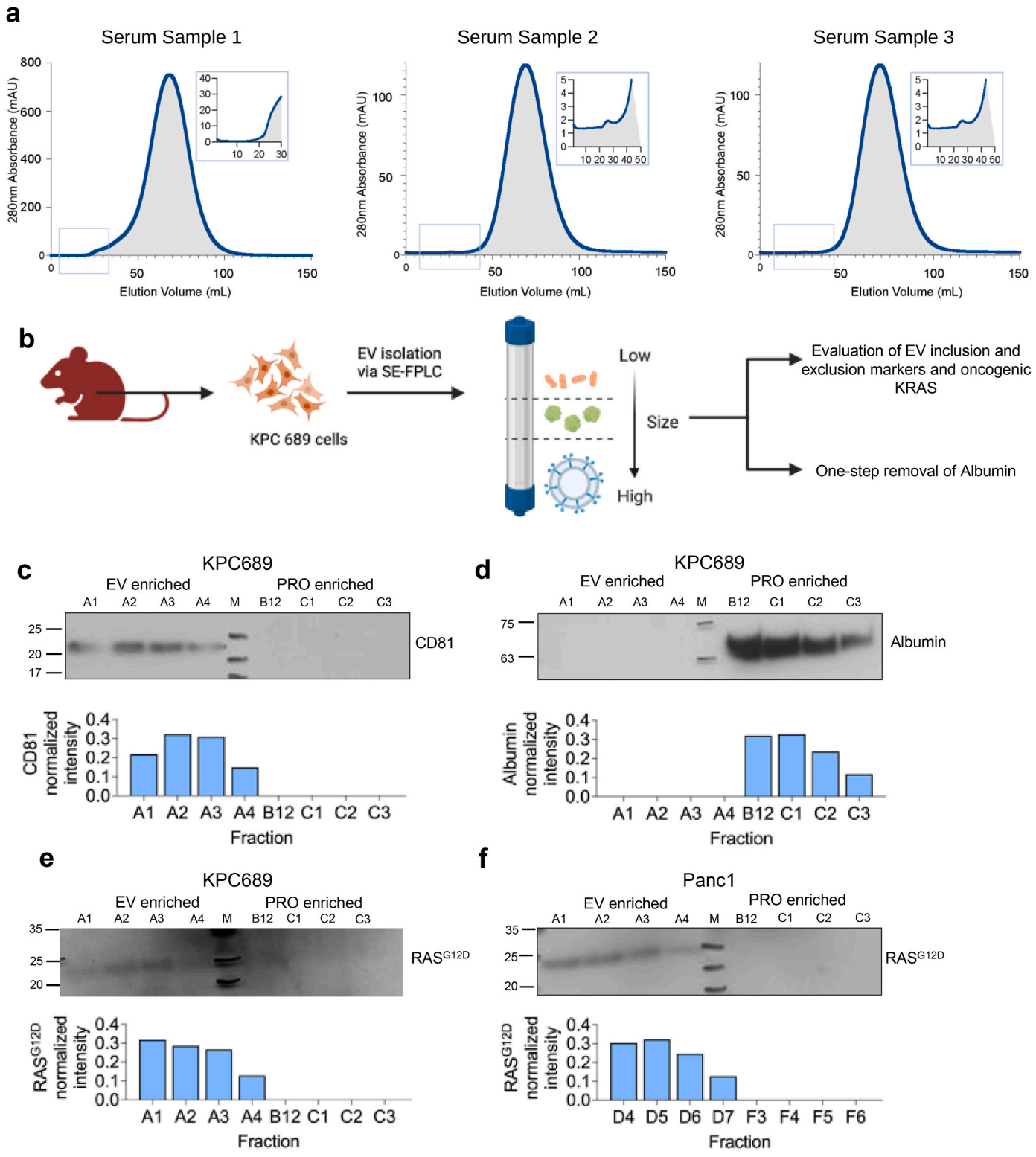

Fig. 4. Validating versatility of SE-FPLC method and detection of mutant KRAS in SE-FPLC isolated EVs. (**A**) UV–Vis chromatographs for EV isolation from serum of n = 3 patients. (**B**) Workflow of EVs isolation from KPC689 mouse PDAC cells. (**C-D**) Equal-sample-volume analysis (45 μL) to study the expression of common EV marker protein (CD81) and EV exclusion marker albumin and quantification of relative intensity bands in KPC689 derived EVs. The fractions analyzed are indicated above each lane and M denotes the molecular weight marker. Quantification of relative intensity of CD81 bands (**C**) and albumin bands (**D**) in KPC689 derived EVs from the western blots in (**C-D top**) analyzed by ImageJ. (**E-F**) Western blot analysis of EVs isolated from mouse PDAC cells (KPC689, **E**) and human PDAC cells (Panc1, **F**) for $KRAS^{G12D}$ protein. The fractions analyzed are indicated above each lane and M denotes the molecular weight marker. Quantification of relative intensity of the bands was analyzed via ImageJ and is shown below the respective blot. Data are presented as individual values in each plot.

albumin was detected in PRO-enriched fractions (Fig. 4C–D). KRAS mutations are associated with greater than 95 % of PDAC patients with $KRAS^{G12D}$ being the most prevalent subset [49]; thus, we profiled SE-FPLC isolated EVs for mutated KRAS (e.g., $KRAS^{G12D}$) using RAS^{G12D} mutant specific antibodies. We identified $KRAS^{G12D}$ protein in EV-enriched fractions across EVs isolated from both murine and human PDAC cell lines (Fig. 4E–F). We compared our SE-FPLC approach with small column volume SEC and consistently found the presence of oncoprotein $KRAS^{G12D}$ in EV-enriched fractions following SEC isolation (Supplementary Fig. S7A).

3. Discussion

A reliable, scalable, rapid, and pure EV isolation method is a highly sought-after goal in the field to further enhance our understanding of the fundamental biological and translational significance of EVs in health and disease. Here we present SE-FPLC, a platform for fast, high performance EV purification [25,32,50]. The SE-FPLC method enables separation of EVs based on size while maintaining their natural morphology and protein marker characteristics. Moreover, the scalability of this platform makes it a feasible option for large-scale EV isolation from various types and volumes of biofluids. Multiple studies have reported that various EV isolation methods have a tendency to co-purify different subpopulations of EVs due to their different principles [51]. SE-FPLC uses the AKTA pure 25 chromatography system (Cytiva) that is CLIA and good manufacturing practice approved and can be deployed for rapid isolation and clinical biomarker or EV content assessment. Other techniques such as the hydrophobic interaction chromatography and affinity chromatography [52–54], while useful are more limited in scope, as they isolate only a subset of EVs. Our analysis revealed that the EVs isolated through SE-FPLC exhibited high signal intensities for specific EV or putative exosome marker proteins, while demonstrating low signal intensity for selected non-EV associated proteins. These findings underscore the effectiveness of SE-FPLC in achieving efficient and pure isolation of EVs. Furthermore, the automatic operation and fraction collection feature of SE-FPLC guarantee a consistent workflow and reproducible results across various sample types, volumes, and EV concentrations. Thus, SE-FPLC provides a convenient and robust approach for the rapid isolation of EVs with high purity and yield, surpassing current EV purification methods.

By employing SE-FPLC for purification of EVs from different cell line models and serum from patients we show the versatility of our platform. EVs isolated from PDAC cell lines showed enrichment of the mutant oncoprotein $KRAS^{G12D}$ in EV-enriched fractions, indicating the feasibility of SE-FPLC in clinical applications. We have identified certain features that have the potential to enhance the functionality of SE-FPLC in future studies. First, the current form of SE-FPLC is limited to single-column isolation. Multi-column approach can be implemented for generating EVs in a continuous fashion to reach highest productivity at an industrial scale. Second, bioreactor systems and hollow-fiber membranes can be utilized for concentrating and filtering cell culture conditioned media for the large-scale production of EVs. Third, the integration of SE-FPLC with downstream detection and analysis technologies such as automated capillary western blot, immunoassays, and quantitative PCR would be advantageous for fast and seamless enrichment and investigation of EVs. Additionally, it is essential to optimize the isolation workflows tailored to the characteristics of each specific sample type. SE-FPLC uses the AKTA pure 25 chromatography system which is CLIA and good manufacturing practice approved and can be deployed for rapid isolation and clinical biomarker or EV content assessment. Our findings presented here complement those of a previously published study [55], which employed tangential flow filtration (TFF) prior to SE-FPLC to concentrate extracellular vesicles (EVs). The combined use of TFF and SE-FPLC yielded comparable results, demonstrating that EVs isolated via SE-FPLC from various cell lines maintained high CD9 expression and exhibited size distributions characteristic of small EVs. However, our research compares this novel method with traditional EV isolation techniques and demonstrates the superior purity obtained with SE-FPLC.

To summarize, we introduce the SE-FPLC methodology for efficient and rapid isolation of EVs with high purity and yield from both cell line models and biofluids, which has the potential to accelerate EV research in life sciences and facilitate translation to clinical applications. The scalability of our approach, enabled by the capability to process large sample volumes and the potential for automation, makes it attractive for industrial applications.

4. Materials and methods

4.1. Cell culture

The cell lines employed in our study (HEK 293T, Panc1, and BJ fibroblasts) were obtained from American Type Culture Collection (ATCC) and T3M4 was obtained from the cell bank at RIKEN BioResource. HEK 293T, Panc1, BJ Fibroblasts and T3M4 cell lines were validated by the Cytogenetics and Cell Authentication Core at MD Anderson. The KPC689 PDAC cancer cell line was isolated from a pancreatic tumor of a $Pdx1^{cre/+}$; $LSL\text{-}Kras^{G12D/+}$; $LSL\text{-}Trp53^{R172H/+}$ (KPC) mouse as described previously [56]. Bone marrow derived MSCs were obtained from Cell Therapy Laboratory at the University of Texas at MD Anderson Center. For HEK 293T and BJ fibroblasts, the culture media was DMEM (Corning) supplemented with 10 % fetal bovine serum (FBS) (Gemini) and 1 % penicillin-streptomycin (Corning). For T3M4, Panc1, and KPC689 the culture media was RPMI 1640 (Corning) supplemented with 10 % FBS and 1 % penicillin-streptomycin. MSCs were cultured in alpha MEM (Corning #10-012-CV) supplemented with 2 U/mL heparin (Sigma H3149–100KU), 1 % L-glutamine (Corning #25-005-CI), 1 % Pen-Strep (Corning #30-002-CI), 1 % non-essential amino acid (NEAA) (Corning #11140050), and 5 % PLT Max (EMD Millipore #SCM141). The doubling time for the cell lines employed in our study are as follows: 49.9 ± 4.2 h for bone marrow derived MSCs, ~56 h for Panc1 cells, ~31–35 h for T3M4 cells and ~33 h for HEK293T cells. All cell lines were seeded at a cell density of 6 x 10^6 cells/flask in 7 T-225cm^2 flasks and cultured to 80 % confluency prior to preparing for EV isolation as described below. All the cell lines were routinely tested for mycoplasma contamination using the LookOut Mycoplasma PCR detection kit (Product no. #MP0035 Sigma-Aldrich) and confirmed negative and maintained in humidified cell culture incubators at 37 °C and 5 % CO_2.

4.2. EV production

Cultured cells at a confluency of about 80 % were thoroughly washed with PBS and subjected to serum-free medium (growth media lacking FBS or PLTMax) for 48 h 30 mL of conditioned medium (CM) was harvested from 7 T to 225cm^2 flasks (total harvest volume 210 mL) and subjected to low gravity (g) centrifugation steps: 400×*g* for 10 min to pellet cells. Supernatant was centrifuged at 2000×*g* for 20 min to remove cellular debris and apoptotic bodies. Next, the CM was filtered using a 0.2 μm pore size filter flask (Fisher Scientific) to select for EVs below 200 nm and further remove cellular debris and apoptotic bodies. After the initial processing, extracellular vesicles were isolated using different isolation methods as detailed below. For all experiments, once the conditioned media (CM) was harvested, all the pre-concentration steps were performed right after CM harvesting. The concentrated CM (CCM) was stored in −80 °C for no more than 48 h, albeit we did not evaluate if long term storage at −80 °C impacts SE-FPLC isolation. After SE-FPLC isolation of the CCM, the SE-FPLC fractions were freshly concentrated, and the looped fractions were stored at −80 °C until the various biophysical and biochemical downstream analysis were performed.

4.3. EV isolation

Four isolation techniques were employed for EV purification: Size Exclusion – Fast Protein Liquid Chromatography (SE-FPLC), OptiPrep – Density Gradient (DG), differential Ultracentrifugation (dUC) and Size Exclusion Chromatography (SEC).

4.3.1. Size exclusion – fast protein liquid chromatography (SE – FPLC)

All separation and purification steps were performed on the AKTA pure 25 chromatography system (Cytiva) equipped with the following components with Cytiva numbers, injection valve (V9-inj), sample pump (S9) with 7 port inlet, Inlet A(V9-IA), and Inlet B (V9-IB). Active monitoring parts were multi-wavelength UV monitor (U9-M), conductivity meter (C9) and pH meter (V9-pH). The UV monitor measured absorbance in the UV/Vis range from 190 nm to 700 nm. The 280 nm wavelength was chosen to evaluate the purification performance and process. The flexible fraction collector (F9–C) that contains cassettes for 96 deep-well plate was applied for all the fractions. The purifications were facilitated by using UNICORN software version 7.3.

After filtration the CM was concentrated using a sterilized Amicon Ultra-15 10 kDa filter following the manufacturer's protocol. The FPLC-compatible column qEV 10 IZON was attached to the FPLC system and then washed with 0.22-μm pore size membrane filtered 20 % ethanol and distilled water. Next the column was equilibrated with Buffer A (phosphate-buffered saline 1x) for 5 column volumes (CVs). In order to clean the sample loop, the procedure was the following to avoid sample going directly to the waste: 1) chose the system in "load", wash the sample loop with PBS using a syringe with volume capacity larger than the loop. 5 ml syringe was selected and left to the injection port. 2) Switch system to "inject", detached the wash syringe and put the sample syringe in the injection port, avoid pushing the plunger. 3) Change the system to "load" and slowing push the plunger of sample syringe. 4) Switch the system back to "Inject". The concentrated conditioned media were applied and loaded to the column. The column was washed with 1.5 CVs of 1X PBS. The peak fractionation (2 mL) was gathered by the 96 deep well plates using the F9–C fraction collector. EV elution peak and non-vesicular matter elution peak were further confirmed by measuring the absorbance of the fractions in real-time by a multiwavelength UV monitor (U9-M). The western blot analysis was carried out for EV inclusion and exclusion markers on the FPLC fractions and the number of particles and total protein in each fraction were determined. In short, equal volumes of collected fractions (45 μL) were subjected to western blotting. The EV-enriched SE-FPLC fractions were further concentrated using the sterilized Amicon Ultra-10 100 kDa filter and EV morphology and size were confirmed by high resolution cryogenic electron microscopy imaging. The FPLC running buffer (Buffer A) consisted of potassium dihydrogen phosphate (0.144 g/L), sodium chloride (9 g/L), disodium phosphate (0.795 g/L) at pH 7.3 to 7.5. The recommended parameters and pre- and post-isolation volumes for SE-FPLC are listed in Table 1. The schematic workflow of the process used for isolation of EVs within the AKTA pure system is outlined in Supplementary Fig. 8.

4.3.2. Size exclusion chromatography (SEC)

After filtration, the CM was concentrated using a sterilized Amicon Ultra-15 10 kDa filter. 500 μL of concentrated CM (CCM) was overlaid on 70 nm qEV 500 size exclusion columns (Izon, SP1) for separation. A dedicated column was used for each cell line, and each column was used up to its recommended limit based on the manufacturer's instructions. The column was flushed in between samples using filtered PBS and filtered 20 % ethanol. For each EV sample, twenty-four fractions of 500 μL were collected using the Izon automated fraction collector (AFC v1). The fractions F7 to F20 were analyzed by western blot to probe for EV-enriched and non-EV enriched fractions. The EV-rich fractions were F7–F10 and non-EV enriched fractions were F15-30. Pooled fractions (7-10) and (11–30) were then concentrated using 10 kDa cutoff filters (Amicon Ultra-15, Millipore). Each fraction was subjected to protein

Table 1
Recommended parameters and pre- and post-isolation volumes for EV isolation.

Isolation Method	Reporting recommendation parameter	Parameter Value
Differential Ultracentrifugation (dUC)	Centrifuge Speed and time	100,000×*g* for 3 h
	Rotor type	SW32 Ti and SW41 Ti (Beckman Coulter)
	Time of centrifugation	3 h
	Tube type	38.5 mL or 13.5 mL Open-Top Ultra Clear round bottom tubes (Beckman Coulter)
	Sample Volume in tube	35 mL (SW32 Ti) and 12 mL (SW41 Ti)
	Temperature during centrifugation	4 °C
	Pre and post-isolation volumes:	Pre-isolation: 210 mL; Post-isolation: 600 μL
Density Gradient (DG)	Density Material	Iodixanol – low osmolarity, non-ionic iodinated density gradient material
	Buffer composition	1x PBS buffer
	Method of gradient/ cushion preparation	OptiPrep gradients were prepared using PBS with specific percentages and volumes for each gradient: 12 % (2 mL), 18 % (2.5 mL), 24 % (2.5 mL), 30 % (2.5 mL) and 36 % (2.5 mL). The EVs were mixed with the OptiPrep medium to achieve a final concentration of 36 % and were loaded at the bottom of a 13.5 mL ultracentrifuge tube.
	Centrifugation speed and time	120,000×*g* for 15 h→ 12 fractions of 1 mL each are collected and labeled as F1 to F12 from top to bottom of the tube. Each fraction is then washed in PBS with a 12-fold dilution and subjected to ultracentrifugation at 120,000 g for 4 h.
	Rotor Type	SW41 Ti rotor from Beckman Coulter
	Temperature during centrifugation	4 °C
	Pre and post-isolation volumes:	Pre-isolation: 210 mL; Post-isolation: 100 μL per fraction
Size Exclusion Chromatography (SEC)	Column Type	IZON qEV Original 500 μL, Gravity flow
	Reuse and storage	Up to 5 times, Storage at 4 °C with 20 % EtOH
	Pre-concentration steps	Sterilized Amicon Ultra-15 10 kDa filter
	Buffer composition	Potassium dihydrogen phosphate (0.144 g/L), Sodium chloride (9 g/L), Disodium phosphate (0.795 g/L) at pH 7.3 to 7.5.
	Pre-isolation volume:	12 mL
	Number of fractions collected	24
	Volume of collected fractions	500 μL
	Post-SEC concentration	The EV-rich fractions are F7–F10 and non-EV enriched fractions are F15-30. Pooled fractions (7-10) and (11–30) are then concentrated using 10 kDa cutoff filters (Amicon

(*continued on next page*)

Table 1 (*continued*)

Isolation Method	Reporting recommendation parameter	Parameter Value
		Ultra-15, Millipore). F1-6 is considered void volume.
Size Exclusion – Fast Protein Liquid Chromatography (SE-FPLC)	Instrumentation	AKTA pure 25 chromatography system (Cytiva)
	Pumps and collection devices	Chromatography system was equipped with the following Cytiva numbers, injection valve (V9-inj), sample pump (S9) with 7 port inlet, Inlet A (V9-IA), and Inlet B (V9-IB). Active monitoring parts were multi-wavelength UV monitor (U9-M), conductivity meter (C9) and pH meter (V9-pH). The UV monitor measured absorbance in the UV/Vis range from 190 nm to 700 nm.
	Fraction Collector	Automated flexible fraction collector (F9–C) that contains cassettes for 96 deep-well plate was applied for all the fractions. The purifications were facilitated by using UNICORN software version 7.3.
	Pre-concentration steps	Performed using sterilized Amicon Ultra-15 10 kDa filter for larger volumes like conditioned media. Amicon Ultra-2 10 kDa filter for smaller volumes like serum or plasma samples.
	Buffer composition	Buffer A and Buffer B: Potassium dihydrogen phosphate (0.144 g/L), Sodium chloride (9 g/L), Disodium phosphate (0.795 g/L) at pH 7.3 to 7.5.
	Pre-isolation volume:	88 mL
	Number of fractions collected	44
	Volume of collected fractions	2 mL
	Flow rates and Pressure	5 mL/min when loading sample onto the column. 8–10 mL/min when performing column regeneration or column wash. Column Pressure – 5–8 psi which corresponds to 0.03 MPa–0.05 MPa Used the working pressure well within the upper limits of the column and the AKTA FPLC system.

concentration measurement, Nanoparticle Tracking Analysis (NTA) and western blot analysis following manufacturer's instructions. The EV-enriched fractions (F7–F10) were further concentrated using sterilized Amicon Ultra-15 10 kDa filter analyzed by high-resolution cryogenic electron microscopy. The recommended parameters and pre- and post-isolation volumes for SEC are listed in Table 1.

4.3.3. Differential ultracentrifugation (dUC)

For EVs isolation by dUC method, harvested conditioned media was subjected to ultracentrifugation at 100,000×*g* for 3 h at 4 °C using a SW32 Ti Beckman Coulter rotor. After ultracentrifugation, the supernatant was discarded, and the EV pellet was resuspended in PBS. For performing cryogenic electron microscopic imaging, EVs were washed in PBS by ultracentrifugation at 100,000×*g* for 3 h at 4 °C in a SW41 Ti rotor (Beckman Coulter). For MSC EVs isolation, the CM was subjected to ultracentrifugation (Sorvall WX 100+ ultracentrifuge) at 100,000×*g* for 3 h at 4 °C using a ThermoFisher T-647.5 rotor. The recommended parameters and pre- and post-isolation volumes for dUC are listed in Table 1.

4.3.4. Density gradient (DG)

EVs that were isolated by UC (1 mL) were further purified using a density gradient purification employing OptiPrep medium (Sigma Aldrich). OptiPrep gradients were prepared using PBS with specific percentages and volumes for each gradient: 12 % (2 mL), 18 % (2.5 mL), 24 % (2.5 mL), 30 % (2.5 mL) and 36 % (2.5 mL). The EVs were mixed with the OptiPrep medium to achieve a final concentration of 36 % and were loaded at the bottom of a 13.5 mL ultracentrifuge tube. The subsequent gradient fractions were gently layered on top in descending order: 30 %, 24 %, 18 % and finally 12 %. The gradients were then ultracentrifuged at 120,000×*g* for 15 h using SW41 Ti rotor from Beckman Coulter. The following day, 12 fractions of 1 mL each were collected and labeled as F1 to F12 from top to bottom of the tube. Each fraction was then washed in PBS with a 12-fold dilution and subjected to ultracentrifugation at 120,000 g for 4 h. Subsequently all the fractions were resuspended in PBS and the EV rich fractions (F1–F6) were utilized for cryogenic electron microscopy imaging and NTA analysis. The recommended parameters and pre- and post-isolation volumes for DG are listed in Table 1.

4.3.5. Column reuse and storage

The columns utilized in this study can be re-used up to 5 times. Columns were re-used based on manufacturer's recommendations for re-usage. To re-use the column, proper re-generation steps were followed between each run using the following experimental protocol to re-generate the column between each run: (1) wash the column with 1.5 column volume (CV) of 1x FPLC running buffer which consisted of potassium dihydrogen phosphate (0.144 g/L), sodium chloride (9 g/L), disodium phosphate (0.795 g/L) at pH 7.3 to 7.5 and (2) 1 CV of 20 % ethanol was used to rinse and store the column. Proper storage of the column between use is essential to prevent contamination and maintain the column performance. To remove excessive contamination between runs it is crucial to perform column performance monitoring. Over time, the efficiency of the column may decrease due to fouling or degradation of the serum/sample in use. The column performance was monitored between runs by analyzing the UV–Vis characteristics between each run. Before running the serum sample through the column, a blank sample (i.e, buffer without serum) was run through the UV–Vis spectrophotometer which is built-into the AKTA FPLC set up to establish a baseline spectrum in this step. The serum sample is then passed through for separation between EVs and other contaminating proteins such as albumin. The absorbance was compared at 280 nm before and after passing the serum through the column to determine the efficiency of albumin removal. After each sample, the column was regenerated according to the aforementioned steps and a blank sample was run through the column after regeneration to measure its UV–Vis spectrum to check for residual contaminants.

4.4. Serum samples

Serum samples from healthy participants were considered deidentified discarded material and exempt from requiring approval from the Institutional Review Board (IRB) of University of Texas at MD Anderson Center, and informed consent was obtained from all participants. Serum samples were collected from each participant, and relevant information can be found in Supplementary Table 1. Each serum sample was centrifuged at 400g for 10 min followed by 2000g for 20 min at 4 °C. The resulting supernatant was then filtered through a 0.22 μm pore size

syringe filter followed by SE-FPLC EV isolation. Post SE-FPLC EV-enriched fractions were combined using a Amicon Ultra-15 100 kDa cutoff concentration filter and serum EVs were subjected to high resolution cryogenic electron microscopy characterization.

4.5. NTA

The concentration and the size distribution of the EVs was measured based on their Brownian motion using a Nano Sight LM10 (Malvern) with a blue 488 nm laser and a highly sensitive sCMOS camera. During measurements, temperature was set and kept constant at 25 °C. For each acquisition, a 90 s delay followed by three captures of 30 s each was employed. The average values of three captures were used to determine the nanoparticle concentration and the mode and mean of the size distribution.

4.6. Western blot analysis

For western blotting EVs were loaded on 4–12 % precast polyacrylamide mini gels (Invitrogen) for electrophoretic separation of proteins. Protein transfer was performed on methanol-activated polyvinylidene fluoride (PVDF) membranes by Trans-Blot Turbo Transfer system (1704150; Bio-Rad). After transfer the membranes were blocked in 5 % BSA in TBS with 0.1 % Tween-20 for 1 h at room temperature. After blocking, the membrane was incubated in primary antibody overnight at 4 °C on a shaker. Next day, secondary antibodies were incubated for 1 h at room temperature. All the primary and secondary antibodies and their concentrations used are listed in Table 2. Post-primary and secondary antibody incubations, the membranes were washed with TBS containing 0.1 % Tween-20 on a shaker, three times at 10 min intervals. The visualization of the membrane was performed with West-Q Pico ECL solution (GenDEPOT) following the manufacturer's instructions. Amersham Hyperfilm (Cytiva) was used for capturing the chemiluminescent signals. All the unprocessed and uncropped scans of blots are provided in Supplementary Data. Blots were quantified in ImageJ and the peak area of a given fraction normalized to the total peak area for all bands on the respective blot.

4.7. Cryogenic transmission electron microscopy

EVs were washed and resuspended in 50 μL of 1x PBS with a minimum concentration of 5.5e10 EV/50 μL. Quanti-foil mesh grids and Lacey Carbon only (400 Mesh Cu) grids were glow discharged for 120 s just before the vitrification step. During vitrification, approximately 3–5 μL of the EVs samples were applied on to the grids, blot time was optimized for 2–5 s, blotting force was optimized between (1–4) to obtain good-quality EV film and followed by snap freezing into liquid ethane using the FEI Vitrobot Mark IV system. The frozen grids were placed in a cryo specimen holder and then transferred to liquid nitrogen for the examination. The samples were imaged using a JEOL 2010 Cryo-TEM (200 kV, LaB6 filament), with a Gatan 626 cooling holder operated at −180 °C. Mini Dose System (MDS) were used for image processing. The DM4 images obtained were converted to TIF and further image analysis was performed. Custom Python codes were utilized for quantifying the segmented EVs for size distribution, length of major and minor axis and eccentricity of the particles as previously described [57].

Table 2
Antibodies used for western blot analysis.

Protein Target	Host species	Dilution	Vendor and Cat. No.
Syntenin - 1	Rabbit	1:2000	Abcam, ab133267
CD81	Mouse	1:1000	Santa Cruz, sc-166029
GAPDH HRP-conjugated	Rabbit	1:1000	Cell Signaling Technology, 8884
Histone H3	Rabbit	1:1000	Abcam, ab201456
Syntenin - 1	Rabbit	1:1000	Abcam, ab19903
GM130	Rabbit	0.2 μg/mL	Sigma Aldrich, G7295
CD9	Rabbit	1:1000	Abcam, ab263019
Albumin	Rabbit	1:1000	Cell Signaling Technology, 4929
RAS^{G12D}	Rabbit	1:1000	Cell Signaling Technology, 14429
Apolipoprotein A1	Rabbit	1:1000	Abcam, ab52945
Anti-mouse HRP-conjugated	–	1:5000	R&D, HAF007
Anti-rabbit HRP-conjugated	–	1:5000	Cell Signaling Technology, 7074

4.8. Statistics

Prism 9.2.0 software was used for graphical representation and statistical analysis. The error bars in the graphical data represent mean ± standard deviation unless otherwise noted in the figure legends. Normal distribution was assessed using the Shapiro-Wilk test.

For comparison of two groups, statistical significance was determined using an unpaired two-tailed *t*-test. One-way ANOVA with Dunnett's multiple comparisons test for datasets with equal variance or Brown-Forsythe and Welch ANOVA with Dunnett's T3 multiple comparisons test for datasets with unequal variance were employed for comparisons of three or more groups. Value of $p < 0.05$ indicated statistical significance. The tests used to determine the statistical significance are indicated in the figure legends.

Data availability

The main data supporting the results of this study are available within the manuscript and supplementary information files. The raw data files are available for research purposes from the corresponding author upon reasonable request. Source data are provided with this paper.

Code availability

Custom Python scripts used for quantifying cryogenic electron microscopic images are available from the corresponding author upon reasonable request.

Ethics approval and consent to participate

Serum samples from healthy participants were considered deidentified discarded material and exempt from requiring approval from the Institutional Review Board (IRB) of University of Texas at MD Anderson Center, and informed consent was obtained from all participants.

CRediT authorship contribution statement

Kshipra S. Kapoor: Writing – review & editing, Writing – original draft, Visualization, Software, Methodology, Investigation, Conceptualization. **Kristen Harris:** Investigation. **Kent A. Arian:** Investigation. **Lihua Ma:** Investigation. **Beatriz Schueng Zancanela:** Investigation. **Kaira A. Church:** Writing – review & editing, Investigation. **Kathleen M. McAndrews:** Writing – review & editing, Methodology, Data curation, Conceptualization. **Raghu Kalluri:** Writing – review & editing, Writing – original draft, Supervision, Resources, Funding acquisition, Conceptualization.

Declaration of competing interest

The authors declare the following financial interests/personal relationships which may be considered as potential competing interests: Raghu Kalluri reports financial support was provided by Fifth Generation. Raghu Kalluri reports financial support was provided by Sid W.

Richardson Foundation. Raghu Kalluri reports financial support was provided by National Institutes of Health. MD Anderson Cancer Center has licensed patents to PranaX for non-cancer use. MD Anderson Cancer Center and Raghu Kalluri report a relationship with PranaX for non-cancer related activities that includes: consulting or advisory and equity or stocks. If there are other authors, they declare that they have no known competing financial interests or personal relationships that could have appeared to influence the work reported in this paper.

Acknowledgements

This work was supported by a gift from Fifth Generation, Inc. ("Love 'Tito's'") and funds from Sid W. Richardson Foundation. EV work in the Kalluri lab is supported by NCI R35CA263815. KAC is supported by the National Center for Advancing Translational Sciences of the National Institutes of Health under Award Numbers TL1TR003169 and UL1TR003167. The content is solely the responsibility of the authors and does not necessarily represent the official views of the National Institutes of Health. We are grateful to Dr. Wenhua Guo for training KSK on cryogenic electron microscopy and Michelle Kirtley for assistance with serum samples. LM is thankful to the Shared Equipment Authority at Rice University for the support. Graphical figures in this work were created using BioRender.

Appendix A. Supplementary data

Supplementary data to this article can be found online at https://doi.org/10.1016/j.bioactmat.2024.08.002.

References

[1] C.K. Schneider, P. Celis, P. Salmikangas, M.A. Figuerola-Santos, L. D'Apote, O. Oliver-Diaz, I. Büttel, R. Mačiulaitis, J.L. Robert, B. Silva Lima, S. Ruiz, B. Jilma, B. Flamion, L. Racheva Todorova, A. Paphitou, I. Haunerova, M. Clausen, T. Maimets, J.H. Trouvin, E. Flory, A. Tsiftsoglou, B. Sarkadi, K. Gudmundsson, M. O'Donovan, G. Migliaccio, J. Ancans, A. Samuel, J.H. Ovelgönne, M. Hystad, A. Mariusz Fal, A. Stela Moraru, P. Turčáni, R. Zorec, L. Åkerblom, G. Narayanan, A. Kent, F. Bignami, J. George Dickson, D. Niederwieser, Challenges with advanced therapy medicinal products and how to meet them, Nat. Rev. Drug Discov. 9 (3 9) (2010) 195–201, https://doi.org/10.1038/nrd3052.

[2] E.C. Scott, A.C. Baines, Y. Gong, R. Moore, G.E. Pamuk, H. Saber, A. Subedee, M. D. Thompson, W. Xiao, R. Pazdur, V.A. Rao, J. Schneider, J.A. Beaver, Trends in the approval of cancer therapies by the FDA in the twenty-first century, Nat. Rev. Drug Discov. 2023 (2023) 1–16, https://doi.org/10.1038/s41573-023-00723-4.

[3] A. Gottschlich, M. Thomas, R. Grünmeier, S. Lesch, L. Rohrbacher, V. Igl, D. Briukhovetska, M.R. Benmebarek, B. Vick, S. Dede, K. Müller, T. Xu, D. Dhoqina, F. Märkl, S. Robinson, A. Sendelhofert, H. Schulz, Ö. Umut, V. Kavaka, C. A. Tsiverioti, E. Carlini, S. Nandi, T. Strzalkowski, T. Lorenzini, S. Stock, P. J. Müller, J. Dörr, M. Seifert, B.L. Cadilha, R. Brabenec, N. Röder, F. Rataj, M. Nüesch, F. Modemann, J. Wellbrock, W. Fiedler, C. Kellner, E. Beltrán, T. Herold, D. Paquet, I. Jeremias, L. von Baumgarten, S. Endres, M. Subklewe, C. Marr, S. Kobold, Single-cell transcriptomic atlas-guided development of CAR-T cells for the treatment of acute myeloid leukemia, Nat. Biotechnol. 2023 (2023) 1–15, https://doi.org/10.1038/s41587-023-01684-0.

[4] X. Dai, CLASH: large-scale engineering system for the discovery of better CAR T cells, Nat. Rev. Immunol. 2023 (2023) 1, https://doi.org/10.1038/s41577-023-00908-3.

[5] M.L. Davila, R.J. Brentjens, CAR T cell therapy: looking back and looking forward, Nat. Can. (Ott.) 3 (12 3) (2022) 1418–1419, https://doi.org/10.1038/s43018-022-00484-w.

[6] L.A. Rojas, Z. Sethna, K.C. Soares, C. Olcese, N. Pang, E. Patterson, J. Lihm, N. Ceglia, P. Guasp, A. Chu, R. Yu, A.K. Chandra, T. Waters, J. Ruan, M. Amisaki, A. Zebboudj, Z. Odgerel, G. Payne, E. Derhovanessian, F. Müller, I. Rhee, M. Yadav, A. Dobrin, M. Sadelain, M. Łuksza, N. Cohen, L. Tang, O. Basturk, M. Gönen, S. Katz, R.K. Do, A.S. Epstein, P. Momtaz, W. Park, R. Sugarman, A.M. Varghese, E. Won, A. Desai, A.C. Wei, M.I. D'Angelica, T.P. Kingham, I. Mellman, T. Merghoub, J.D. Wolchok, U. Sahin, Ö. Türeci, B.D. Greenbaum, W.R. Jarnagin, J. Drebin, E.M. O'Reilly, V.P. Balachandran, Personalized RNA neoantigen vaccines stimulate T cells in pancreatic cancer, Nature (2023) 144–150, https://doi.org/10.1038/s41586-023-06063-y, 2023 618:7963 618.

[7] A.J. Barbier, A.Y. Jiang, P. Zhang, R. Wooster, D.G. Anderson, The clinical progress of mRNA vaccines and immunotherapies, Nat. Biotechnol. 40 (6 40) (2022) 840–854, https://doi.org/10.1038/s41587-022-01294-2.

[8] F.P. Polack, S.J. Thomas, N. Kitchin, J. Absalon, A. Gurtman, S. Lockhart, J. L. Perez, G. Pérez Marc, E.D. Moreira, C. Zerbini, R. Bailey, K.A. Swanson, S. Roychoudhury, K. Koury, P. Li, W.V. Kalina, D. Cooper, R.W. Frenck, L. L. Hammitt, Ö. Türeci, H. Nell, A. Schaefer, S. Ünal, D.B. Tresnan, S. Mather, P. R. Dormitzer, U. Şahin, K.U. Jansen, W.C. Gruber, Safety and efficacy of the BNT162b2 mRNA covid-19 vaccine, N. Engl. J. Med. 383 (2020) 2603–2615, https://doi.org/10.1056/NEJMOA2034577/SUPPL_FILE/NEJMOA2034577_PROTOCOL.PDF.

[9] L.R. Baden, H.M. El Sahly, B. Essink, K. Kotloff, S. Frey, R. Novak, D. Diemert, S. A. Spector, N. Rouphael, C.B. Creech, J. McGettigan, S. Khetan, N. Segall, J. Solis, A. Brosz, C. Fierro, H. Schwartz, K. Neuzil, L. Corey, P. Gilbert, H. Janes, D. Follmann, M. Marovich, J. Mascola, L. Polakowski, J. Ledgerwood, B.S. Graham, H. Bennett, R. Pajon, C. Knightly, B. Leav, W. Deng, H. Zhou, S. Han, M. Ivarsson, J. Miller, T. Zaks, Efficacy and safety of the mRNA-1273 SARS-CoV-2 vaccine, N. Engl. J. Med. 384 (2021) 403–416, https://doi.org/10.1056/NEJMOA2035389/SUPPL_FILE/NEJMOA2035389_DATA-SHARING.PDF.

[10] R. Kalluri, V.S. LeBleu, The biology, function, and biomedical applications of exosomes, Science (2020) 367, https://doi.org/10.1126/SCIENCE.AAU6977/ASSET/F5050DD7-9124-4A75-9FBE-2BCDF3F27CD8/ASSETS/GRAPHIC/367_AAU6977_F6.JPEG.

[11] D.K. Jeppesen, Q. Zhang, J.L. Franklin, R.J. Coffey, Extracellular vesicles and nanoparticles: emerging complexities, Trends Cell Biol. (2023), https://doi.org/10.1016/J.TCB.2023.01.002, 0.

[12] R. Kalluri, K.M. McAndrews, The role of extracellular vesicles in cancer, Cell 186 (2023) 1610–1626, https://doi.org/10.1016/J.CELL.2023.03.010.

[13] T. Skotland, K. Sandvig, A. Llorente, Lipids in exosomes: current knowledge and the way forward, Prog. Lipid Res. 66 (2017), https://doi.org/10.1016/j.plipres.2017.03.001.

[14] C. Théry, M. Ostrowski, E. Segura, Membrane vesicles as conveyors of immune responses, Nat. Rev. Immunol. 9 (2009), https://doi.org/10.1038/nri2567.

[15] N. Yim, S.W. Ryu, K. Choi, K.R. Lee, S. Lee, H. Choi, J. Kim, M.R. Shaker, W. Sun, J. H. Park, D. Kim, W. Do Heo, C. Choi, Exosome engineering for efficient intracellular delivery of soluble proteins using optically reversible protein-protein interaction module, Nat. Commun. 7 (2016), https://doi.org/10.1038/ncomms12277.

[16] J.P.K. Armstrong, M.N. Holme, M.M. Stevens, Re-engineering extracellular vesicles as smart nanoscale therapeutics, ACS Nano 11 (2017), https://doi.org/10.1021/acsnano.6b07607.

[17] S. Kamerkar, V.S. Lebleu, H. Sugimoto, S. Yang, C.F. Ruivo, S.A. Melo, J.J. Lee, R. Kalluri, Exosomes facilitate therapeutic targeting of oncogenic KRAS in pancreatic cancer, Nature 546 (2017), https://doi.org/10.1038/nature22341.

[18] M.W. Becker, L.D. Peters, T. Myint, D. Smurlick, A. Powell, T.M. Brusko, E. A. Phelps, I M M U N O LO G Y Immune engineered extracellular vesicles to modulate T cell activation in the context of type 1 diabetes. https://www.science.org, 2023.

[19] A. Möller, R.J. Lobb, The evolving translational potential of small extracellular vesicles in cancer, Nat. Rev. Cancer 20 (12 20) (2020) 697–709, https://doi.org/10.1038/s41568-020-00299-w.

[20] Z.G. Zhang, B. Buller, M. Chopp, Exosomes — beyond stem cells for restorative therapy in stroke and neurological injury, Nat. Rev. Neurol. 15 (4 15) (2019) 193–203, https://doi.org/10.1038/s41582-018-0126-4.

[21] J. Park, J.S. Park, C.H. Huang, A. Jo, K. Cook, R. Wang, H.Y. Lin, J. Van Deun, H. Li, J. Min, L. Wang, G. Yoon, B.S. Carter, L. Balaj, G.S. Choi, C.M. Castro, R. Weissleder, H. Lee, An integrated magneto-electrochemical device for the rapid profiling of tumour extracellular vesicles from blood plasma, Nat. Biomed. Eng. 5 (7 5) (2021) 678–689, https://doi.org/10.1038/s41551-021-00752-7.

[22] R. Cecchin, Z. Troyer, K. Witwer, K.V. Morris, Extracellular vesicles: the next generation in gene therapy delivery, Mol. Ther. 31 (2023) 1225–1230, https://doi.org/10.1016/j.ymthe.2023.01.021.

[23] L. Cheng, A.F. Hill, Therapeutically harnessing extracellular vesicles, Nat. Rev. Drug Discov. 21 (5 21) (2022) 379–399, https://doi.org/10.1038/s41573-022-00410-w.

[24] I.K. Herrmann, M.J.A. Wood, G. Fuhrmann, Extracellular vesicles as a next-generation drug delivery platform, Nat. Nanotechnol. 16 (7 16) (2021) 748–759, https://doi.org/10.1038/s41565-021-00931-2.

[25] X. Li, A.L. Corbett, E. Taatizadeh, N. Tasnim, J.P. Little, C. Garnis, M. Daugaard, E. Guns, M. Hoorfar, I.T.S. Li, Challenges and opportunities in exosome research—perspectives from biology, engineering, and cancer therapy, APL Bioeng. 3 (2019) 11503, https://doi.org/10.1063/1.5087122.

[26] J. Van Deun, P. Mestdagh, P. Agostinis, Ö. Akay, S. Anand, J. Anckaert, Z. A. Martinez, T. Baetens, E. Beghein, L. Bertier, G. Berx, J. Boere, S. Boukouris, M. Bremer, D. Buschmann, J.B. Byrd, C. Casert, L. Cheng, A. Cmoch, D. Daveloose, E. De Smedt, S. Demirsoy, V. Depoorter, B. Dhondt, T.A.P. Driedonks, A. Dudek, A. Elsharawy, I. Floris, A.D. Foers, K. Gärtner, A.D. Garg, E. Geeurickx, J. Gettemans, F. Ghazavi, B. Giebel, T.G. Kormelink, G. Hancock, H. Helsmoortel, A.F. Hill, V. Hyenne, H. Kalra, D. Kim, J. Kowal, S. Kraemer, P. Leidinger, C. Leonelli, Y. Liang, L. Lippens, S. Liu, A. Lo Cicero, S. Martin, S. Mathivanan, P. Mathiyalagan, T. Matusek, G. Milani, M. Monguió-Tortajada, L.M. Mus, D. C. Muth, A. Németh, E.N.M. Nolte-'T Hoen, L. O'Driscoll, R. Palmulli, M.W. Pfaffl, B. Primdal-Bengtson, E. Romano, Q. Rousseau, S. Sahoo, N. Sampaio, M. Samuel, B. Scicluna, B. Soen, A. Steels, J.V. Swinnen, M. Takatalo, S. Thaminy, C. Théry, J. Tulkens, I. Van Audenhove, S. Van Der Grein, A. Van Goethem, M.J. Van Herwijnen, G. Van Niel, N. Van Roy, A.R. Van Vliet, N. Vandamme, S. Vanhauwaert, G. Vergauwen, F. Verweij, A. Wallaert, M. Wauben, K.W. Witwer, M.I. Zonneveld, O. De Wever, J. Vandesompele, A. Hendrix, EV-TRACK: transparent reporting and centralizing knowledge in extracellular vesicle research, Nat. Methods 14 (3 14) (2017) 228–232, https://doi.org/10.1038/nmeth.4185.

[27] F. Momen-Heravi, Isolation of extracellular vesicles by ultracentrifugation, Methods Mol. Biol. 1660 (2017) 25–32, https://doi.org/10.1007/978-1-4939-7253-1_3.

[28] N.L. Syn, L. Wang, E.K.H. Chow, C.T. Lim, B.C. Goh, Exosomes in cancer nanomedicine and immunotherapy: prospects and challenges, Trends Biotechnol. 35 (2017) 665–676, https://doi.org/10.1016/j.tibtech.2017.03.004.
[29] J.Z. Nordin, Y. Lee, P. Vader, I. Mäger, H.J. Johansson, W. Heusermann, O.P. B. Wiklander, M. Hällbrink, Y. Seow, J.J. Bultema, J. Gilthorpe, T. Davies, P. J. Fairchild, S. Gabrielsson, N.C. Meisner-Kober, J. Lehtiö, C.I.E. Smith, M.J. A. Wood, S.E.L. Andaloussi, Ultrafiltration with size-exclusion liquid chromatography for high yield isolation of extracellular vesicles preserving intact biophysical and functional properties, Nanomedicine 11 (2015), https://doi.org/10.1016/j.nano.2015.01.003.
[30] Y. Yang, Y. Wang, S. Wei, C. Zhou, J. Yu, G. Wang, W. Wang, L. Zhao, Extracellular vesicles isolated by size-exclusion chromatography present suitability for RNomics analysis in plasma, J. Transl. Med. 19 (2021), https://doi.org/10.1186/s12967-021-02775-9.
[31] Z. Niu, R.T.K. Pang, W. Liu, Q. Li, R. Cheng, W.S.B. Yeung, Polymer-based precipitation preserves biological activities of extracellular vesicles from an endometrial cell line, PLoS One 12 (2017), https://doi.org/10.1371/JOURNAL.PONE.0186534.
[32] E.M. Guerreiro, B. Vestad, L.A. Steffensen, H.C.D. Aass, M. Saeed, R. Øvstebø, D. E. Costea, H.K. Galtung, T.M. Søland, Efficient extracellular vesicle isolation by combining cell media modifications, ultrafiltration, and size-exclusion chromatography, PLoS One 13 (2018), https://doi.org/10.1371/JOURNAL.PONE.0204276.
[33] H.K. Woo, V. Sunkara, J. Park, T.H. Kim, J.R. Han, C.J. Kim, H. Il Choi, Y.K. Kim, Y. K. Cho, Exodisc for rapid, size-selective, and efficient isolation and analysis of nanoscale extracellular vesicles from biological samples, ACS Nano 11 (2017) 1360–1370, https://doi.org/10.1021/ACSNANO.6B06131.
[34] R. Xu, D.W. Greening, H.J. Zhu, N. Takahashi, R.J. Simpson, Extracellular vesicle isolation and characterization: toward clinical application, J. Clin. Invest. 126 (2016) 1152–1162, https://doi.org/10.1172/JCI81129.
[35] M. Wu, Y. Ouyang, Z. Wang, R. Zhang, P.H. Huang, C. Chen, H. Li, P. Li, D. Quinn, M. Dao, S. Suresh, Y. Sadovsky, T.J. Huang, Isolation of exosomes from whole blood by integrating acoustics and microfluidics, Proc. Natl. Acad. Sci. U. S. A. 114 (2017) 10584–10589, https://doi.org/10.1073/PNAS.1709210114.
[36] P. Sharma, S. Ludwig, L. Muller, C.S. Hong, J.M. Kirkwood, S. Ferrone, T. L. Whiteside, Immunoaffinity-based isolation of melanoma cell-derived exosomes from plasma of patients with melanoma, J. Extracell. Vesicles 7 (2018), https://doi.org/10.1080/20013078.2018.1435138.
[37] Y. Chen, Q. Zhu, L. Cheng, Y. Wang, M. Li, Q. Yang, L. Hu, D. Lou, J. Li, X. Dong, L. P. Lee, F. Liu, Exosome detection via the ultrafast-isolation system: exodus, Nat. Methods 18 (2 18) (2021) 212–218, https://doi.org/10.1038/s41592-020-01034-x.
[38] G. Corso, I. Mäger, Y. Lee, A. Görgens, J. Bultema, B. Giebel, M.J.A. Wood, J. Z. Nordin, S. El Andaloussi, Reproducible and scalable purification of extracellular vesicles using combined bind-elute and size exclusion chromatography, Sci. Rep. 7 (2017), https://doi.org/10.1038/s41598-017-10646-x.
[39] P. Li, M. Kaslan, S.H. Lee, J. Yao, Z. Gao, Progress in exosome isolation techniques, Theranostics 7 (2017) 789–804, https://doi.org/10.7150/THNO.18133.
[40] M.Y. Konoshenko, E.A. Lekchnov, A.V. Vlassov, P.P. Laktionov, Isolation of extracellular vesicles: general methodologies and latest trends, BioMed Res. Int. 2018 (2018), https://doi.org/10.1155/2018/8545347.
[41] C. Théry, K.W. Witwer, E. Aikawa, M.J. Alcaraz, J.D. Anderson, R. Andriantsitohaina, A. Antoniou, T. Arab, F. Archer, G.K. Atkin-Smith, D.C. Ayre, J.M. Bach, D. Bachurski, H. Baharvand, L. Balaj, S. Baldacchino, N.N. Bauer, A. A. Baxter, M. Bebawy, C. Beckham, A. Bedina Zavec, A. Benmoussa, A.C. Berardi, P. Bergese, E. Bielska, C. Blenkiron, S. Bobis-Wozowicz, E. Boilard, W. Boireau, A. Bongiovanni, F.E. Borràs, S. Bosch, C.M. Boulanger, X. Breakefield, A.M. Breglio, M. Brennan, D.R. Brigstock, A. Brisson, M.L.D. Broekman, J.F. Bromberg, P. Bryl-Górecka, S. Buch, A.H. Buck, D. Burger, S. Busatto, D. Buschmann, B. Bussolati, E. I. Buzás, J.B. Byrd, G. Camussi, D.R.F. Carter, S. Caruso, L.W. Chamley, Y.T. Chang, A.D. Chaudhuri, C. Chen, S. Chen, L. Cheng, A.R. Chin, A. Clayton, S.P. Clerici, A. Cocks, E. Cocucci, R.J. Coffey, A. Cordeiro-da-Silva, Y. Couch, F.A.W. Coumans, B. Coyle, R. Crescitelli, M.F. Criado, C. D'Souza-Schorey, S. Das, P. de Candia, E. F. De Santana, O. De Wever, H.A. del Portillo, T. Demaret, S. Deville, A. Devitt, B. Dhondt, D. Di Vizio, L.C. Dieterich, V. Dolo, A.P. Dominguez Rubio, M. Dominici, M.R. Dourado, T.A.P. Driedonks, F.V. Duarte, H.M. Duncan, R. M. Eichenberger, K. Ekström, S. El Andaloussi, C. Elie-Caille, U. Erdbrügger, J. M. Falcón-Pérez, F. Fatima, J.E. Fish, M. Flores-Bellver, A. Försönits, A. Frelet-Barrand, F. Fricke, G. Fuhrmann, S. Gabrielsson, A. Gámez-Valero, C. Gardiner, K. Gärtner, R. Gaudin, Y.S. Gho, B. Giebel, C. Gilbert, M. Gimona, I. Giusti, D.C. I. Goberdhan, A. Görgens, S.M. Gorski, D.W. Greening, J.C. Gross, A. Gualerzi, G. N. Gupta, D. Gustafson, A. Handberg, R.A. Haraszti, P. Harrison, H. Hegyesi, A. Hendrix, A.F. Hill, F.H. Hochberg, K.F. Hoffmann, B. Holder, H. Holthofer, B. Hosseinkhani, G. Hu, Y. Huang, V. Huber, S. Hunt, A.G.E. Ibrahim, T. Ikezu, J. M. Inal, M. Isin, A. Ivanova, H.K. Jackson, S. Jacobsen, S.M. Jay, M. Jayachandran, G. Jenster, L. Jiang, S.M. Johnson, J.C. Jones, A. Jong, T. Jovanovic-Talisman, S. Jung, R. Kalluri, S. ichi Kano, S. Kaur, Y. Kawamura, E.T. Keller, D. Khamari, E. Khomyakova, A. Khvorova, P. Kierulf, K.P. Kim, T. Kislinger, M. Klingeborn, D. J. Klinke, M. Kornek, M.M. Kosanović, Á.F. Kovács, E.M. Krämer-Albers, S. Krasemann, M. Krause, I.V. Kurochkin, G.D. Kusuma, S. Kuypers, S. Laitinen, S. M. Langevin, L.R. Languino, J. Lannigan, C. Lässer, L.C. Laurent, G. Lavieu, E. Lázaro-Ibáñez, S. Le Lay, M.S. Lee, Y.X.F. Lee, D.S. Lemos, M. Lenassi, A. Leszczynska, I.T.S. Li, K. Liao, S.F. Libregts, E. Ligeti, R. Lim, S.K. Lim, A. Linē, K. Linnemannstöns, A. Llorente, C.A. Lombard, M.J. Lorenowicz, Á.M. Lörincz, J. Lötvall, J. Lovett, M.C. Lowry, X. Loyer, Q. Lu, B. Lukomska, T.R. Lunavat, S.L. N. Maas, H. Malhi, A. Marcilla, J. Mariani, J. Mariscal, E.S. Martens-Uzunova, L. Martin-Jaular, M.C. Martinez, V.R. Martins, M. Mathieu, S. Mathivanan, M. Maugeri, L.K. McGinnis, M.J. McVey, D.G. Meckes, K.L. Meehan, I. Mertens, V. R. Minciacchi, A. Möller, M. Møller Jørgensen, A. Morales-Kastresana, J. Morhayim, F. Mullier, M. Muraca, L. Musante, V. Mussack, D.C. Muth, K. H. Myburgh, T. Najrana, M. Nawaz, I. Nazarenko, P. Nejsum, C. Neri, T. Neri, R. Nieuwland, L. Nimrichter, J.P. Nolan, E.N.M. Nolte-'t Hoen, N. Noren Hooten, L. O'Driscoll, T. O'Grady, A. O'Loghlen, T. Ochiya, M. Olivier, A. Ortiz, L.A. Ortiz, X. Osteikoetxea, O. Ostegaard, M. Ostrowski, J. Park, D.M. Pegtel, H. Peinado, F. Perut, M.W. Pfaffl, D.G. Phinney, B.C.H. Pieters, R.C. Pink, D.S. Pisetsky, E. Pogge von Strandmann, I. Polakovicova, I.K.H. Poon, B.H. Powell, I. Prada, L. Pulliam, P. Quesenberry, A. Radeghieri, R.L. Raffai, S. Raimondo, J. Rak, M. I. Ramirez, G. Raposo, M.S. Rayyan, N. Regev-Rudzki, F.L. Ricklefs, P.D. Robbins, D.D. Roberts, S.C. Rodrigues, E. Rohde, S. Rome, K.M.A. Rouschop, A. Rughetti, A. E. Russell, P. Saá, S. Sahoo, E. Salas-Huenuleo, C. Sánchez, J.A. Saugstad, M. J. Saul, R.M. Schiffelers, R. Schneider, T.H. Schøyen, A. Scott, E. Shahaj, S. Sharma, O. Shatnyeva, F. Shekari, G.V. Shelke, A.K. Shetty, K. Shiba, P.R.M. Siljander, A. M. Silva, A. Skowronek, O.L. Snyder, R.P. Soares, B.W. Sódar, C. Soekmadji, J. Sotillo, P.D. Stahl, W. Stoorvogel, S.L. Stott, E.F. Strasser, S. Swift, H. Tahara, M. Tewari, K. Timms, S. Tiwari, R. Tixeira, M. Tkach, W.S. Toh, R. Tomasini, A. C. Torrecilhas, J.P. Tosar, V. Toxavidis, L. Urbanelli, P. Vader, B.W.M. van Balkom, S.G. van der Grein, J. Van Deun, M.J.C. van Herwijnen, K. Van Keuren-Jensen, G. van Niel, M.E. van Royen, A.J. van Wijnen, M.H. Vasconcelos, I.J. Vechetti, T. D. Veit, L.J. Vella, É. Velot, F.J. Verweij, B. Vestad, J.L. Viñas, T. Visnovitz, K. V. Vukman, J. Wahlgren, D.C. Watson, M.H.M. Wauben, A. Weaver, J.P. Webber, V. Weber, A.M. Wehman, D.J. Weiss, J.A. Welsh, S. Wendt, A.M. Wheelock, Z. Wiener, L. Witte, J. Wolfram, A. Xagorari, P. Xander, J. Xu, X. Yan, M. Yáñez-Mó, H. Yin, Y. Yuana, V. Zappulli, J. Zarubova, V. Žėkas, J. ye Zhang, Z. Zhao, L. Zheng, A.R. Zheutlin, A.M. Zickler, P. Zimmermann, A.M. Zivkovic, D. Zocco, E. K. Zuba-Surma, Minimal information for studies of extracellular vesicles 2018 (MISEV2018): a position statement of the International Society for Extracellular Vesicles and update of the MISEV2014 guidelines, J. Extracell. Vesicles 7 (2018), https://doi.org/10.1080/20013078.2018.1535750.
[42] F.G. Kugeratski, K. Hodge, S. Lilla, K.M. McAndrews, X. Zhou, R.F. Hwang, S. Zanivan, R. Kalluri, Quantitative proteomics identifies the core proteome of exosomes with syntenin-1 as the highest abundant protein and a putative universal biomarker, Nat. Cell Biol. 23 (2021), https://doi.org/10.1038/s41556-021-00693-y.
[43] Y. Yuana, J. Levels, A. Grootemaat, A. Sturk, R. Nieuwland, Co-isolation of extracellular vesicles and high-density lipoproteins using density gradient ultracentrifugation, J. Extracell. Vesicles 3 (2014), https://doi.org/10.3402/JEV.V3.23262.
[44] Q. Zhang, D.K. Jeppesen, J.N. Higginbotham, J.L. Franklin, R.J. Coffey, Comprehensive isolation of extracellular vesicles and nanoparticles, Nat. Protoc. 18 (5 18) (2023) 1462–1487, https://doi.org/10.1038/s41596-023-00811-0.
[45] Q. Zhang, D.K. Jeppesen, J.N. Higginbotham, R. Graves-Deal, V.Q. Trinh, M. A. Ramirez, Y. Sohn, A.C. Neininger, N. Taneja, E.T. McKinley, H. Niitsu, Z. Cao, R. Evans, S.E. Glass, K.C. Ray, W.H. Fissell, S. Hill, K.L. Rose, W.J. Huh, M. K. Washington, G.D. Ayers, D.T. Burnette, S. Sharma, L.H. Rome, J.L. Franklin, Y. A. Lee, Q. Liu, R.J. Coffey, Supermeres are functional extracellular nanoparticles replete with disease biomarkers and therapeutic targets, Nat. Cell Biol. 23 (12 23) (2021) 1240–1254, https://doi.org/10.1038/s41556-021-00805-8.
[46] K. Li, D.K. Wong, F.S. Luk, R.Y. Kim, R.L. Raffai, Isolation of plasma lipoproteins as a source of extracellular RNA, Methods Mol. Biol. 1740 (2018) 139–153, https://doi.org/10.1007/978-1-4939-7652-2_11.
[47] D.L. Michell, R.M. Allen, S.R. Landstreet, S. Zhao, C.L. Toth, Q. Sheng, K.C. Vickers, Isolation of high-density lipoproteins for non-coding small RNA quantification, J. Vis. Exp. 2016 (2016), https://doi.org/10.3791/54488.
[48] S.A. Melo, L.B. Luecke, C. Kahlert, A.F. Fernandez, S.T. Gammon, J. Kaye, V. S. LeBleu, E.A. Mittendorf, J. Weitz, N. Rahbari, C. Reissfelder, C. Pilarsky, M. F. Fraga, D. Piwnica-Worms, R. Kalluri, Glypican-1 identifies cancer exosomes and detects early pancreatic cancer, Nature (2015) 177–182, https://doi.org/10.1038/nature14581, 2015 523:7559 523.
[49] D.P. Ryan, T.S. Hong, N. Bardeesy, Pancreatic adenocarcinoma, 1039–1049, https://doi.org/10.1056/NEJMRA1404198, 2014.
[50] W. Wang, J. Luo, S. Wang, Recent progress in isolation and detection of extracellular vesicles for cancer diagnostics, Adv. Healthcare Mater. 7 (2018), https://doi.org/10.1002/ADHM.201800484.
[51] B. Mateescu, E.J.K. Kowal, B.W.M. van Balkom, S. Bartel, S.N. Bhattacharyya, E. I. Buzás, A.H. Buck, P. de Candia, F.W.N. Chow, S. Das, T.A.P. Driedonks, L. Fernández-Messina, F. Haderk, A.F. Hill, J.C. Jones, K.R. Van Keuren-Jensen, C. P. Lai, C. Lässer, I. di Liegro, T.R. Lunavat, M.J. Lorenowicz, S.L.N. Maas, I. Mäger, M. Mittelbrunn, S. Momma, K. Mukherjee, M. Nawaz, D.M. Pegtel, M.W. Pfaffl, R. M. Schiffelers, H. Tahara, C. Théry, J.P. Tosar, M.H.M. Wauben, K.W. Witwer, E.N. M. Nolte-'t Hoen, Obstacles and opportunities in the functional analysis of extracellular vesicle RNA - an ISEV position paper, J. Extracell. Vesicles 6 (2017), https://doi.org/10.1080/20013078.2017.1286095.
[52] T.F. Bruce, T.J. Slonecki, L. Wang, S. Huang, R.R. Powell, R.K. Marcus, Exosome isolation and purification via hydrophobic interaction chromatography using a polyester, capillary-channeled polymer fiber phase, Electrophoresis 40 (2019), https://doi.org/10.1002/elps.201800417.
[53] J. Zhu, J. Zhang, X. Ji, Z. Tan, D.M. Lubman, Column-based technology for CD9-HPLC immunoaffinity isolation of serum extracellular vesicles, J. Proteome Res. 20 (2021), https://doi.org/10.1021/acs.jproteome.1c00549.
[54] B. Barnes, T. Caws, S. Thomas, A.P. Shephard, R. Corteling, P. Hole, D. G. Bracewell, Investigating heparin affinity chromatography for extracellular

vesicle purification and fractionation, J. Chromatogr. A 1670 (2022), https://doi.org/10.1016/j.chroma.2022.462987.
[55] C. Keysberg, H. Schneider, K. Otte, Production cell analysis and compound-based boosting of small extracellular vesicle secretion using a generic and scalable production platform, Biotechnol. Bioeng. 120 (2023), https://doi.org/10.1002/bit.28322.
[56] X. Zheng, J.L. Carstens, J. Kim, M. Scheible, J. Kaye, H. Sugimoto, C.C. Wu, V. S. Lebleu, R. Kalluri, Epithelial-to-mesenchymal transition is dispensable for metastasis but induces chemoresistance in pancreatic cancer, Nature 527 (2015) 525–530, https://doi.org/10.1038/NATURE16064.
[57] K.S. Kapoor, S. Kong, H. Sugimoto, W. Guo, V. Boominathan, Y.-L. Chen, S. L. Biswal, T. Terlier, K.M. McAndrews, R. Kalluri, Single extracellular vesicle imaging and computational analysis identifies inherent architectural heterogeneity, ACS Nano (2024), https://doi.org/10.1021/acsnano.3c12556.